



**HAL**  
open science

## Induced exchange bias in NiMn/CoFe multilayer thin films sputtered on a quartz substrate by field cooling

Charles Mauc, Thomas Perrier, Johan Moulin, Patrick Kayser

### ► To cite this version:

Charles Mauc, Thomas Perrier, Johan Moulin, Patrick Kayser. Induced exchange bias in NiMn/CoFe multilayer thin films sputtered on a quartz substrate by field cooling. *Journal of Magnetism and Magnetic Materials*, 2022, 544, pp.168649. 10.1016/j.jmmm.2021.168649 . hal-03618866

**HAL Id: hal-03618866**

**<https://hal.science/hal-03618866>**

Submitted on 24 Mar 2022

**HAL** is a multi-disciplinary open access archive for the deposit and dissemination of scientific research documents, whether they are published or not. The documents may come from teaching and research institutions in France or abroad, or from public or private research centers.

L'archive ouverte pluridisciplinaire **HAL**, est destinée au dépôt et à la diffusion de documents scientifiques de niveau recherche, publiés ou non, émanant des établissements d'enseignement et de recherche français ou étrangers, des laboratoires publics ou privés.

# Induced exchange bias in NiMn/CoFe multilayer thin films sputtered on a quartz substrate by field cooling

Charles Mauc <sup>a, b, \*</sup>, Thomas Perrier <sup>a</sup>, Johan Moulin <sup>b</sup>, Patrick Kayser <sup>a</sup>

<sup>a</sup> ONERA – The French Aerospace, Physics and Instrumentation Department, 39 avenue de la Division Leclerc, 92320 Châtillon, France

<sup>b</sup> C2N, Microsystems and nanobiofluidic Department, 10 boulevard Thomas Gobert, 91120 Palaiseau, France

\*Contact: [charles.mauc@onera.fr](mailto:charles.mauc@onera.fr) ; ORCID: <https://orcid.org/0000-0002-9181-3829>

## 1. Introduction

Many applications rely on materials with specific magnetic properties. For example, RF components need strong anisotropy [1] [2], magneto-resistive read heads use a ferromagnetic layer which has to be perfectly pinned [3] [4], and some MEMS actuators and sensors exploit a ferromagnetic layer with a global magnetic moment as high as possible [5] [6] [7].

In the specific case of MEMS magnetic sensors, ongoing works are conducted on the design and realization of quartz MEMS resonant structures dedicated to measure one component of the earth magnetic field [25 $\mu$ T; 65 $\mu$ T] and meant to be integrated into magneto-inertial cells [8] [9]. Previous works show that the sensitivity of this kind of magnetometers is directly correlated with the intensity and the direction of the macroscopic magnetic moment  $\vec{m}$  of the magnetic material(s) being used [9]. To work efficiently, we aim for  $\|\vec{m}\|$  to be steady on [-1mT; 1mT] to stabilize the sensitivity and as high as possible to maximise it. Furthermore,  $\vec{m}$  needs to be in one direction to avoid cross-axis measurement. Moreover, for the specifications of the sensor not to be environment dependant,  $\vec{m}$  should be insensitive to temperature or magnetic shocks.

In this article, we will present how we use the exchange anisotropy appearing at the interface between ferromagnetic (FM) and antiferromagnetic (AFM) thin films to achieve the objectives. In this way, the influence of the annealing temperature, the thickness of the films and the shape anisotropy have been studied.

## 2. Materials and process

Soft FM materials despite their high saturation magnetization have low coercive field so their magnetization is easily reversible. On the other hand, the magnetization of hard FM materials is stable relatively to the external magnetic field but they are very sensitive to ambient temperature and their internal stress is crippling to be used

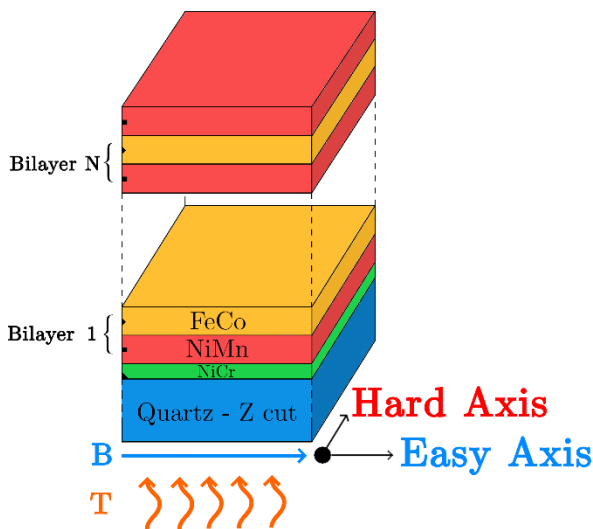


Figure 2: NiMn/FeCo multilayer stack on a quartz substrate during field cooling procedure

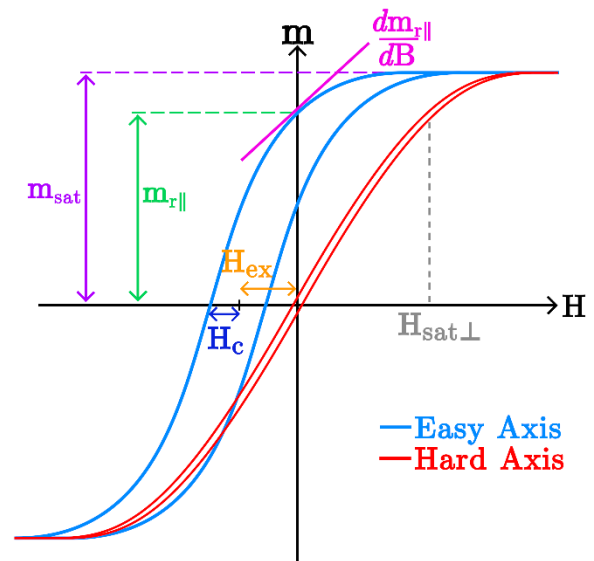


Figure 1: Hysteresis loops in the easy axis and the hard axis of a multilayer FM/AFM after a field cooling procedure

in thin film [7] [10] [11]. As a workaround, the introduction of exchange anisotropy appearing at the interfaces between a FM and AFM thin films after a field cooling procedure (Figure 2) will shift the hysteresis cycle along the *easy axis* (notation:  $\parallel$ ) by  $H_{ex}$ : the exchange field (Figure 1) [12]. Stacking thin AFM/FM bilayers over themselves could therefore lead to a high remanent moment close to the saturation moment and almost constant on the desired range [-1mT; 1mT] along the *easy axis*. To avoid cross-axis measurements from the sensor, it is also necessary to reduce to sensitivity of the magnetic moment to a transverse magnetic field along the *hard axis* (notation:  $\perp$ ) which is in the thin film plane and perpendicular to the *easy axis* (Figure 2). That is why we will consider the following parameters and objectives (Figure 1):

- $m_{r\parallel} \geq 10 \mu\text{A} \cdot \text{m}^2$       – the remanent magnetic moment along the *easy axis*
- $\frac{m_{r\parallel}}{m_{sat}} \rightarrow 100\%$       – the proportion of magnetic moment along the *easy axis at null field*
- $\left. \frac{dm_{\parallel}}{dB} \right|_{B=0} = \frac{dm_{r\parallel}}{dB} \rightarrow 0 \mu\text{A} \cdot \text{m}^2$       – the sensitivity to small fields along the *easy axis*
- $H_{sat\perp}$  as high as possible      – the saturation field in the *hard axis* which corresponds to the maximum of  $\frac{\partial^2 m_{\perp}}{\partial H^2}$

### 2.1. Choice of the FM and AFM materials

**Ferromagnetic material** ( $\text{Co}_{35}\text{Fe}_{65}$ ): Cobalt iron alloys exhibit ferromagnetic properties. They are well known to have one of the highest saturation magnetization at room temperature ( $> 2.4 \text{ T}$ ) [13] [14], high Curie temperature (920-1000K) [15] [16] and low coercive field ( $< 10\text{mT}$ ) [17]. They are also easy to deposit with a magnetron-sputtering machine. Among those alloys, the  $\text{Co}_{35}\text{Fe}_{65}$  is the one that has the best-suited properties to reach the objectives [17].

**Antiferromagnetic material** ( $\text{Ni}_{50}\text{Mn}_{50}$ ): AFMs suited for exchange bias applications have been extensively studied in the literature [12]. The NiMn is rather special among the other AFMs because of its Neel temperature  $T_N \approx 1000 \text{ K}$  far above its blocking temperature  $T_B \approx 700\text{K}$ . It has a great exchange energy ( $J_{ex} = 50 \text{ nJ}/\text{cm}^2$ ) [17] [18] and is stable with regard to the temperature [18]. However, the minimum thickness of NiMn to have enough exchange bias is about 25-30nm [19] [20] [21].

We chose this multilayer: [Quartz (001) (**500  $\mu\text{m}$** ) + NiCr (**20 nm**) + [NiMn/ CoFe] $_{10}$  + NiMn] (Figure 2). The NiCr underlayer provides a great adherence between the quartz substrate and the first NiMn layer and the extra layer of NiMn helps to fully pin the last CoFe layer.  $\text{Ni}_{80}\text{Cr}_{20}$ , NiMn and CoFe have been deposited with a magnetron-sputtering machine ( $p_{Ar} = 1.7 \text{ mbar}$ ,  $P = 200\text{W}$ ) on individual  $3000\mu\text{m} \times 3000\mu\text{m} \times 500\mu\text{m}$  quartz (001) samples.

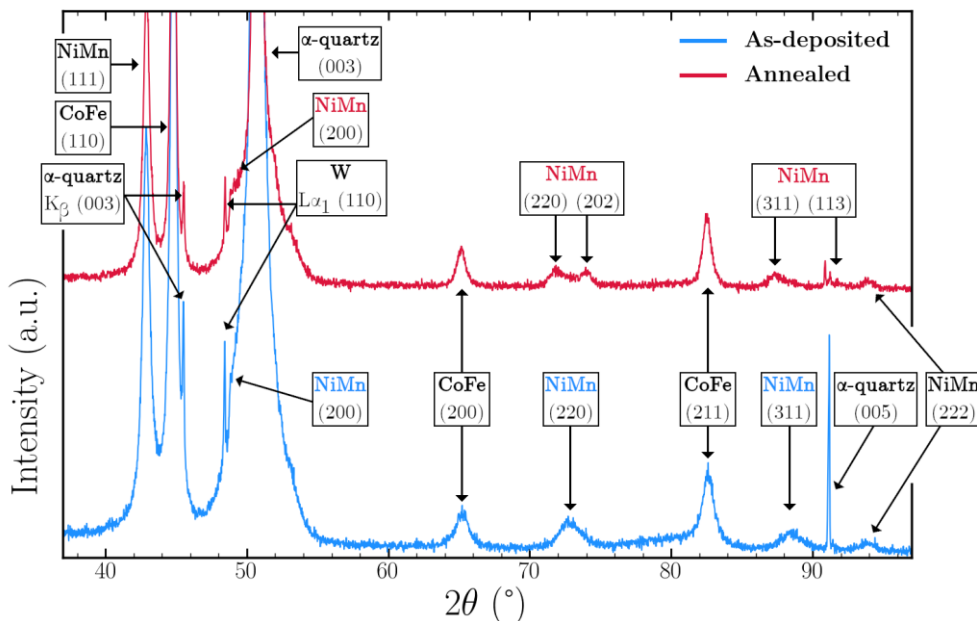


Figure 3. XRD diagrams of as-deposited and annealed CoFe/NiMn stack

## 2.2. Annealing procedure

The classic field cooling procedure for FM/AFM takes place in the presence of a static magnetic field  $\vec{B}$  which sets the direction of the *easy axis* [12]. In the temperature range  $[T_N; T_C]$ , the AFM becomes paramagnetic. Therefore, the AFM and FM spins can easily align with  $\vec{B}$ . When cooling below  $T_N$ , the AFM becomes antiferromagnetic again and its spins are aligned with FM spins. Thanks to the coupling between the spins at the interface, an additional torque applies on the FM spins [12] [22]. The external field has to overcome it in order to reverse the magnetization, explaining the shift of the hysteresis loop (Figure 1).

The NiMn deposited with the magnetron-sputtering machine has an A1 structure which is paramagnetic. To transform it into the antiferromagnetic  $L_10$  structure, an annealing procedure is necessary. We can observe this transformation thanks to a comparison between the X-Ray Diffraction (XRD) diagrams of the as-deposited and annealed CoFe/NiMn stack (Figure 3). Indeed, some NiMn peaks are splitting or shifting, which is a distinctive feature of the transformation of a cubic structure into a quadratic structure [23] [24], while the  $\alpha$ -quartz and CoFe do not change.

Consequently, for the exchange bias to appear for the couple FeCo/NiMn, we do not need to follow the classic field cooling procedure. Indeed, most of CoFe's spins align with  $\vec{B}$  because it has a relatively small coercive field, and for the reason that at the beginning the annealing procedure the NiMn did not transform yet, the average direction of its spins will be along  $\vec{B}$  too. The exchange anisotropy then appears as NiMn switch into its antiferromagnetic phase. That is why there is no need to set the temperature above  $T_N$ , making this procedure efficient at low temperature compare to the classic field cooling procedure for NiMn. The annealing procedure, set to last 300 min, has been done under high vacuum ( $\approx 10^{-6}$ mbar), under a magnetic field of 20mT.

## 3. Influence of the chosen parameters on the macroscopic magnetization

### 3.1. Effect of the annealing temperature

The transition of NiMn from its paramagnetic phase to the antiferromagnetic one must be as complete as possible. To characterize the correct annealing temperature, exchange bias must appear, and the exchange field  $H_{ex}$  must be higher than the coercive field  $H_c$ . As expected,  $H_{ex}$  is almost null without annealing and an high value (5.8 mT) is obtained after annealing at 275°C (Figure 4 and Figure 5) which is consistent with [25]–[27]. It was not possible to anneal higher than 275°C because of the limitations of the oven. All the following results corresponds to samples annealed at 275°C.

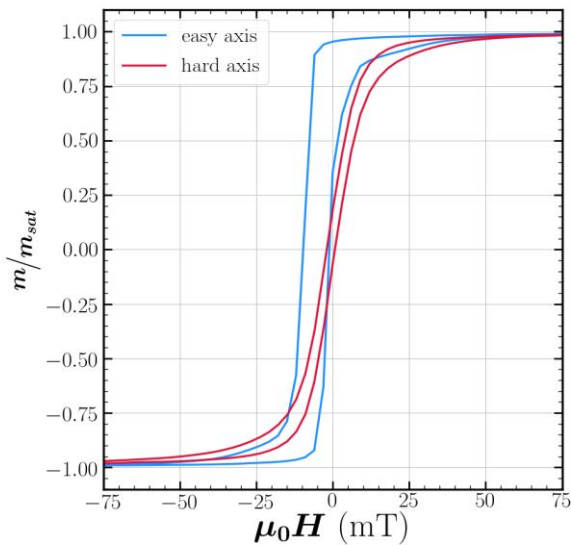


Figure 4. Hysteresis loops along the easy axis and hard axis for the multilayer quartz + NiCr (20nm) + [NiMn (50nm) / CoFe (50nm)]<sub>10</sub> + NiMn (50nm) annealed at 275°C

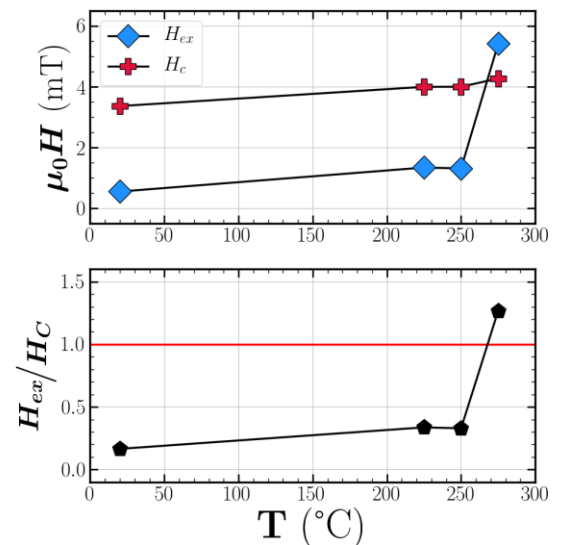


Figure 5: Exchange and coercive fields over temperature for the multilayer quartz + NiCr (20nm) + [NiMn (50nm) / CoFe (50nm)]<sub>10</sub> + NiMn (50nm).

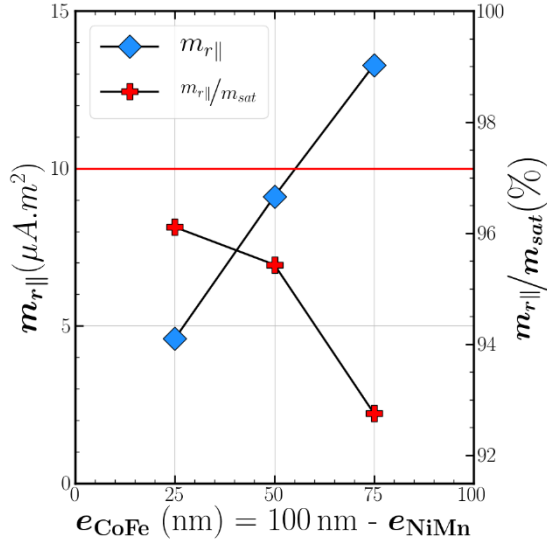


Figure 6:  $m_{r||}$  and  $m_{r||}/m_{\text{sat}}$  in function of  $e_{\text{CoFe}}$  for the multilayer quartz + NiCr (20nm) + [NiMn (50nm) / CoFe (50nm)]<sub>10</sub> + NiMn (50nm).

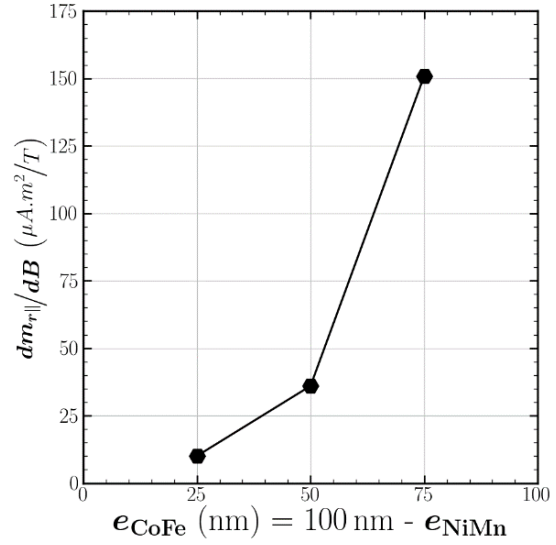


Figure 7:  $\frac{dm_{r||}}{dB}$  in function of  $e_{\text{CoFe}}$  for the multilayer quartz + NiCr (20nm) + [NiMn (50nm) / CoFe (50nm)]<sub>10</sub> + NiMn (50nm).

### 3.2. Effect of the thickness of CoFe

We decided to set the thickness of the NiMn/FeCo bilayer to 100 nm. Therefore, when the thickness of CoFe increases, the thickness of NiMn decreases. On one hand, the increase of  $m_{r||}$  from 4.6 to 13.3  $\mu\text{A}\cdot\text{m}^2$  is easily explained by the fact that it only depends on the quantity of CoFe (Figure 6). On the other hand, when  $e_{\text{NiMn}}$  diminishes, the exchange bias lowers. In consequence, the hysteresis cycle is less shifted. That is the reason why  $\frac{m_{r||}}{m_{\text{sat}}}$  (Figure 6) decreases down from 96 to 93% and  $\frac{dm_{r||}}{dB}$  (Figure 7) increases up from 10 to 150  $\mu\text{A}\cdot\text{m}^2/\text{T}$ . The best compromise between high magnetization and low sensitivity to small magnetic field is for  $e_{\text{CoFe}} = e_{\text{NiMn}} = 50\text{nm}$ .

### 3.3. Effect of shape anisotropy

Additionally with the exchange anisotropy, we decided to introduce shape anisotropy to favour the direction of  $\vec{m}$  along the *easy axis*, which is perpendicular to the direction of the sensor sensitivity. The aim is to reduce the influence of a magnetic field along the *hard axis* on the magnetic moment.

We conceived a specific process to induce shape anisotropy by patterning the film in stripes (Figure 8 and Figure 9). It is compatible with the chemical etching of quartz substrates because it needs to be integrated in the full sensor fabrication process. All the process steps are carried out on the entire wafer that gathers many quartz samples. They are “separated” from each other thanks to the step n°4 of the Figure 9. Then, the stripes are obtained thanks to a lift-off technique after the deposition of the magnetic multilayer. During the annealing, the magnetic field is applied along the length of the stripes.

The stripes will be referred by their aspect ratio  $R = \frac{\text{length}}{\text{width}}$ . They all have the same length ( $l = 3000\mu\text{m}$ ) but have different widths ( $w = 9$  to  $2800\mu\text{m}$ ) leading to an aspect ratio ranging from 1 to 333. Moreover, each stripe is pulled apart from its neighbour from a specific distance  $h = 30\mu\text{m}$ .

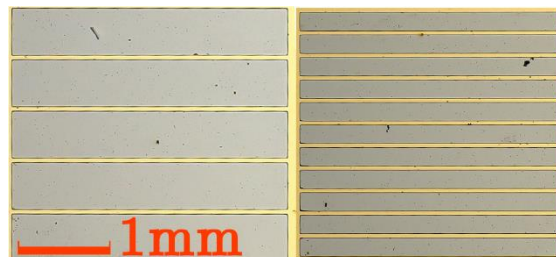


Figure 8: Examples of productions.

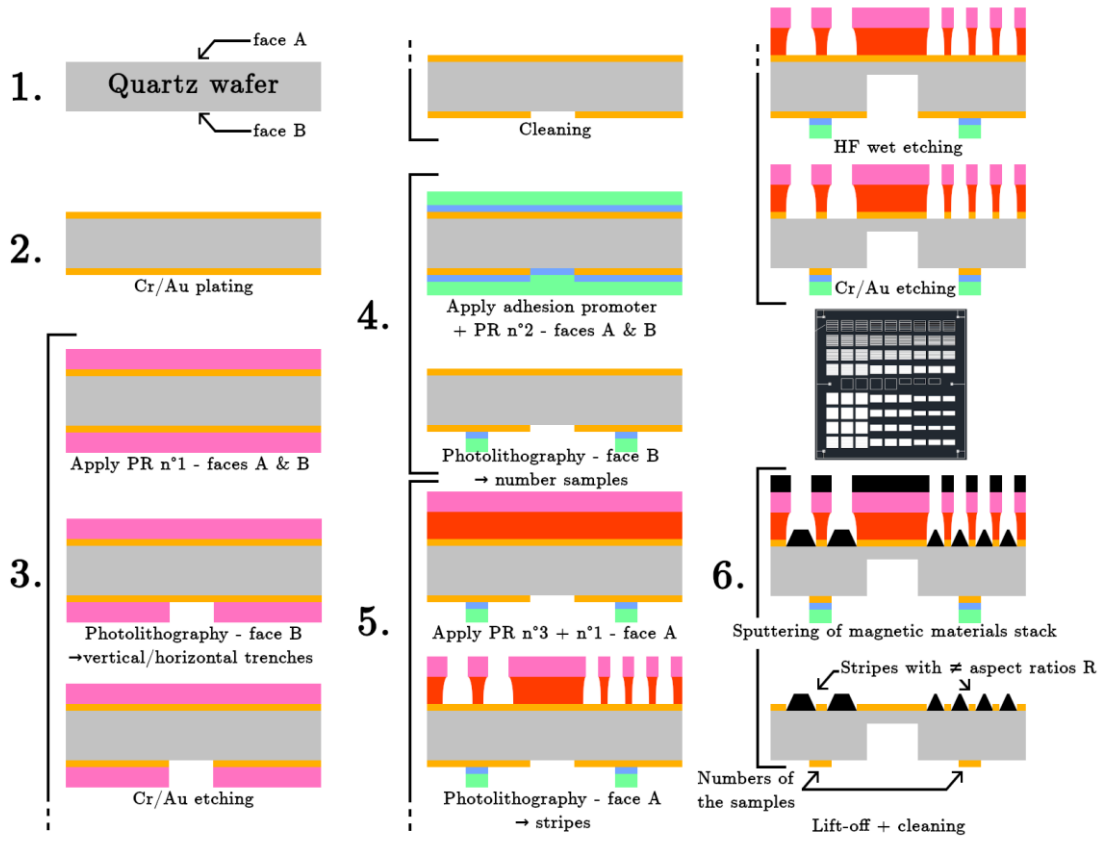


Figure 9: Process to make stripes out of NiMn/CoFe multilayer.

When we observe the hysteresis cycles in the *easy axis*, we can notice a *shouldering* (Figure 11) which does not appear in the *hard axis* (Figure 10). It may be caused by one missing NiMn layer or by the NiCr layer that change the local crystallography of the first NiMn layer, preventing it to be in the L<sub>1</sub>0 antiferromagnetic structure.

When the aspect ratio  $R$  increases, the *emptiness* (proportion of surface with no magnetic materials) does not increase linearly. It reaches 75% for  $R = 333.3$  because the gap is constant, explaining the decrease of  $m_{r||}$  from 7.9 to 2.1  $\mu\text{A}\cdot\text{m}^2$  (Figure 14).

We can notice the increase of the saturation field  $H_{sat}$  in the *hard axis* from 5mT up to 88mT (Figure 15) which illustrates the rise of the demagnetizing field [10] [28]. In consequence, the hysteresis loops appear much flatter

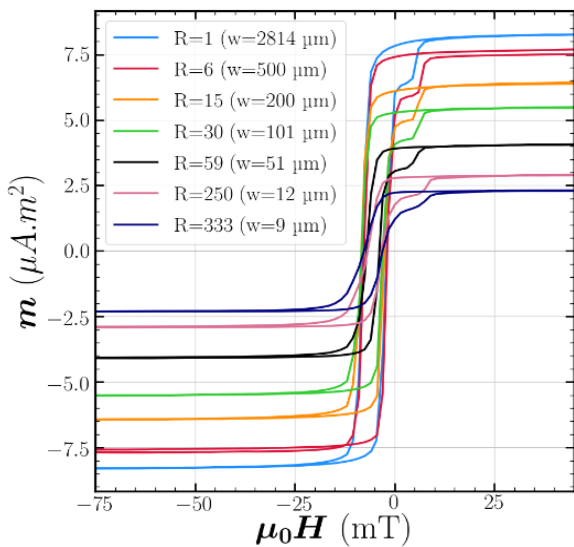


Figure 11: Hysteresis loops for different aspect ratios in the easy axis

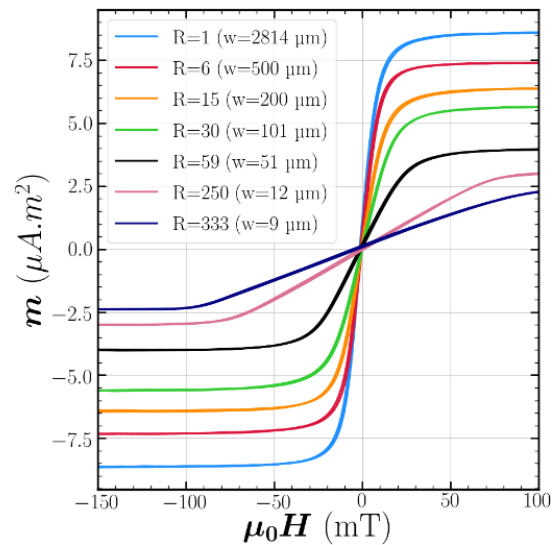


Figure 10: Hysteresis loops for different aspect ratios in the hard axis in the plane of the thin film

in the *hard axis* (Figure 10). Moreover, considering the fact that  $\frac{m_{r\parallel}}{m_{sat}}$  is roughly constant at 95% (Figure 13), it reveals that the decrease  $\frac{dm_{r\parallel}}{dB}$  (Figure 12) is due to the decrease of  $m_{r\parallel}$ .

It demonstrates that the introduction of stripes lessen the sensitivity of the sensor with the decrease of  $m_{r\parallel}$ , that this range aspect ratios does not favour the *easy axis* as the privileged direction for  $\vec{m}$ , however, the sensitivity of the  $\vec{m}$  to a magnetic field in the *hard axis* greatly lessens. It may be necessary to have closer and thinner stripes to avoid the downsides.

## Conclusion

The annealing temperature, the thickness of the materials and the shape anisotropy can remarkably influence the magnetic properties of a CoFe/NiMn multilayer sputtered on a quartz substrate. Indeed, the annealing temperature can make the exchange bias appears or not. The thicknesses of CoFe and NiMn determine the strength of the exchange bias. In addition, with the introduction of shape anisotropy, it is conceivable with thinner and closer

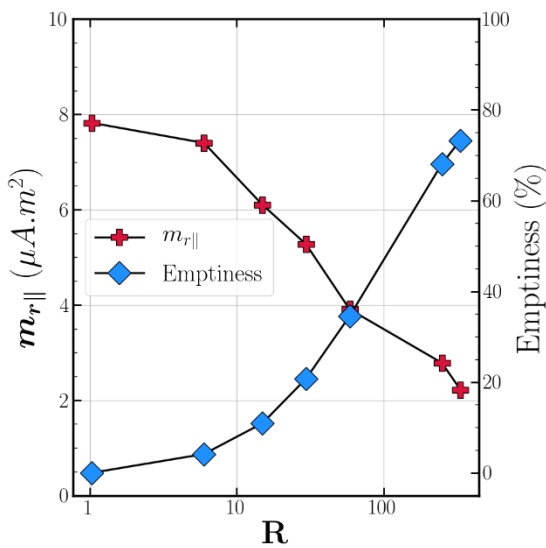


Figure 14. Remanent magnetic moment and emptiness in function of the aspect ratio

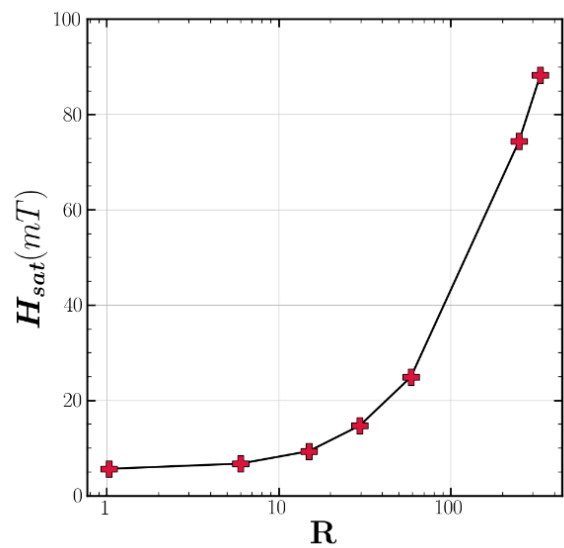


Figure 15: Saturation field for the hard axis in function of the aspect ratio.

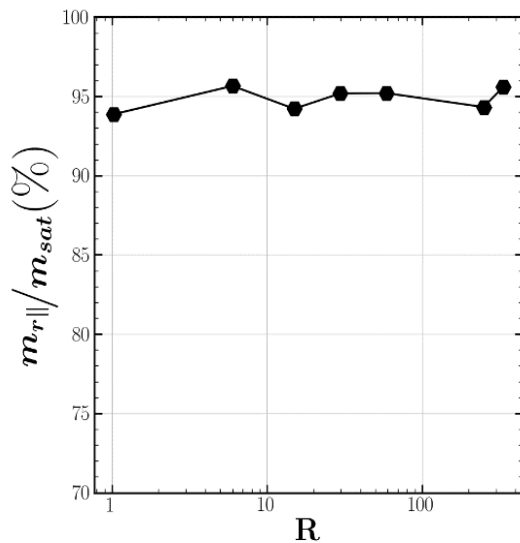


Figure 13. Proportion of magnetic moment in the easy axis

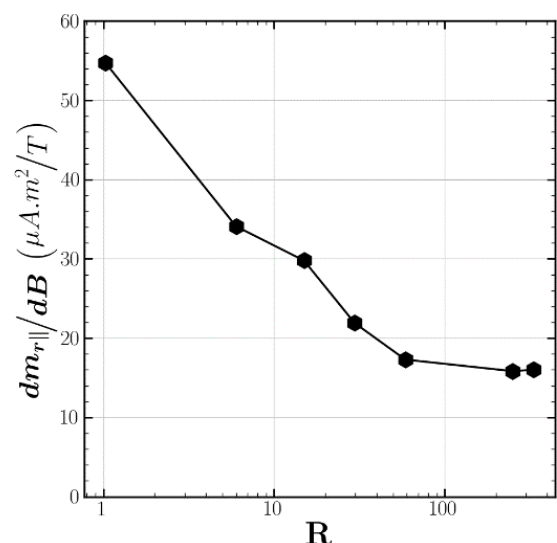


Figure 12:  $\frac{dm_{r\parallel}}{dB}$  in function of strip aspect ratio

stripes to notably reduce the sensitivity of the  $\vec{m}$  to a magnetic field in the *hard axis* and favour a direction for  $\vec{m}$  without lowering the sensor sensitivity.

## Acknowledgement

This work was supported by the French ANR program Astrid Maturation (ANR-19-ASMA-0002-01) led by the French Ministry of Army (DGA), under the contract “MAGRIT II”.

## References

- [1] B. Orlando, A.-S. Royet, Y. Lamy, and B. Viala, “Evaluation of Exchange-Biased Magnetic Materials for High Density GHz Toroidal Integrated Inductors,” *J. Magn. Soc. Japan*, vol. 30, no. 6–1, pp. 519–522, 2006.
- [2] Y. Lamy and B. Viala, “NiMn, IrMn, and NiO exchange coupled CoFe multilayers for microwave applications,” *IEEE Trans. Magn.*, vol. 42, no. 10, pp. 3332–3334, 2006.
- [3] E. E. Fullerton and J. R. Childress, “Spintronics, Magnetoresistive Heads, and the Emergence of the Digital World,” *Proc. IEEE*, vol. 104, no. 10, pp. 1787–1795, Oct. 2016.
- [4] L. Jogschies *et al.*, “Recent developments of magnetoresistive sensors for industrial applications,” *Sensors (Switzerland)*, vol. 15, no. 11, pp. 28665–28689, 2015.
- [5] J. E. Lenz, “A Review of Magnetic Sensors,” *Proc. IEEE*, vol. 78, no. 6, pp. 973–989, 1990.
- [6] P. Ripka and M. Janosek, “Advances in Magnetic Field Sensors,” *IEEE Sens. J.*, vol. 10, no. 6, pp. 1108–1116, Jun. 2010.
- [7] D. Ettelt, “Conception et fabrication d’un magnétomètre à jauge de contrainte,” Université de Grenoble, 2012.
- [8] R. Levy, T. Perrier, P. Kayser, B. Bourgeteau, and J. Moulin, “A micro-resonator based magnetometer,” *Microsyst. Technol.*, vol. 23, no. 9, pp. 3937–3943, 2017.
- [9] T. Perrier, R. Levy, P. Kayser, B. Verlhac, and J. Moulin, “Modeling of a vibrating MEMS magnetometer partially covered with a ferromagnetic thin film,” *5th IEEE Int. Symp. Inert. Sensors Syst. Inert. 2018 - Proc.*, pp. 1–4, 2018.
- [10] E. Du Trémolet de Lacheisserie, *Magnetism I - Fondements*, Grenoble S. 1999.
- [11] J. Y. Wang, D. K. Sood, M. K. Ghantasala, and N. Dytlewski, “Characterization of sputtered SmCo thin films for light element contamination using RBS and HIERDA techniques,” *Vacuum*, vol. 75, no. 1, pp. 17–23, 2004.
- [12] J. Nogués *et al.*, “Exchange bias in nanostructures,” *Phys. Rep.*, vol. 422, no. 3, pp. 65–117, 2005.
- [13] B. R. Craig, S. McVitie, J. N. Chapman, A. B. Johnston, and D. O. O’Donnell, “Transmission electron microscopy study of CoFe films with high saturation magnetization,” *J. Appl. Phys.*, vol. 100, no. 5, 2006.
- [14] D. S. Schmool and D. Markó, “Magnetism in Solids: Hysteresis,” in *Reference Module in Materials Science and Materials Engineering*, Elsevier, 2018.
- [15] W. Nursiyanto, L. Rohman, M. Alfatun N., and E. Purwandari, “THE EFFECT OF COBALT CONTENT ON MAGNETIC PROPERTIES OF CoFe ALLOYS,” *Spektra J. Fis. dan Apl.*, vol. 5, no. 2, pp. 87–96, 2020.
- [16] R. S. Sundar and S. C. Deevi, “Soft magnetic FeCo alloys: Alloy development, processing, and properties,” *Int. Mater. Rev.*, vol. 50, no. 3, pp. 157–192, 2005.
- [17] Y. Lamy, “Matériaux magnétiques doux hétérogènes à combinaison d’aimantation élevée et de grande anisotropie utilisant le couplage d’échange, pour des applications microondes,” Université de Limoges, 2006.
- [18] J. P. Nozières, S. Jaren, Y. B. Zhang, A. Zeltser, K. Pentek, and V. S. Speriosu, “Blocking temperature distribution and long-term stability of spin-valve structures with Mn-based antiferromagnets,” *J. Appl. Phys.*, vol. 87, no. 8, pp. 3920–3925, 2000.
- [19] A. J. Devasahayam, K. R. Mountfield, and M. H. Kryder, “Small track width MR sensors stabilized with NiMn,” *IEEE Trans. Magn.*, vol. 33, no. 5 PART 1, pp. 2881–2883, 1997.
- [20] S. Mao, N. Amin, and E. Murdock, “Temperature dependence of giant magnetoresistance properties of NiMn pinned spin valves,” *J. Appl. Phys.*, vol. 83, no. 11, pp. 6807–6809, 1998.
- [21] M. F. Toney, M. G. Samant, T. Lin, and D. Mauri, “Thickness dependence of exchange bias and structure in MnPt and MnNi spin valves,” *Appl. Phys. Lett.*, vol. 81, no. 24, pp. 4565–4567, 2002.
- [22] W. H. Meiklejohn and C. P. Bean, “New Magnetic Anisotropy,” *Phys. Rev.*, vol. 102, no. 5, pp. 1413–1414, Jun. 1956.
- [23] T. Lin, D. Mauri, N. Staud, C. Hwang, J. K. Howard, and G. L. Gorman, “Improved exchange coupling between ferromagnetic Ni-Fe and antiferromagnetic Ni-Mn-based films,” *Appl. Phys. Lett.*, vol. 65, no. 9, pp. 1183–1185, 1994.

- [24] M. Huang, "Kinetic study on the phase transformations in sputter deposited NiMn thin films," *J. Appl. Phys.*, vol. 97, no. 6, 2005.
- [25] Y. Lamy and B. Viala, "Combination of ultimate magnetization and ultrahigh uniaxial anisotropy in CoFe exchange-coupled multilayers," *J. Appl. Phys.*, vol. 97, no. 10, pp. 1–4, 2005.
- [26] M. Silva, D. C. Leitao, S. Cardoso, and P. Freitas, "MnNi-based spin valve sensors combining high thermal stability, small footprint and pTesla detectivities," *AIP Adv.*, vol. 8, no. 5, 2018.
- [27] G. Vallejo-Fernandez, T. Dimopoulos, M. Ruehrig, and K. O'Grady, "Annealing effect on thermal stability and microstructure in IrMn / Co60 Fe20 B20 bilayers," *J. Magn. Magn. Mater.*, vol. 310, no. 2 SUPPL. PART 3, pp. 786–788, 2007.
- [28] D. X. Chen, E. Pardo, and A. Sanchez, "Demagnetizing factors of rectangular prisms and ellipsoids," *IEEE Trans. Magn.*, vol. 38, no. 4 II, pp. 1742–1752, 2002.